PNAS
www.pnas.org

Supplementary Information for

Pronounced summer warming in northwest Greenland during the Holocene and Last Interglacial

Jamie M. McFarlin, Yarrow Axford, Magdalena R. Osburn, Meredith A. Kelly, Erich C. Osterberg, Lauren B. Farnsworth

Jamie McFarlin
Email: jamie@earth.northwestern.edu

This PDF file includes:

Supplementary text
Figs. S1 to S5
Tables S1 to S3
References for SI reference citations

www.pnas.org/cgi/doi/10.1073/pnas.1720420115

Supplementary Information Text

Methods

Core Information. Core 14WLL-2A is 216 cm long and was split into two sections (2A-1, 2A-2) in the field for transport and storage. Cores were split and processed at the LacCore National Lacustrine Core Facility at the University of Minnesota. MS was measured every 0.3 cm using a Bartington MS2 meter and MS2E sensor mounted to a Geotek MSCL-XYZ with a sampling time of 10 s. Gamma density was measured with a ^{137}Cesium source and detector mounted to a Geotek MSCL-S every 0.5 cm with a count time of 10 s. Results from sections for which data were not recorded by the instrument or where there is clearly interference in the measurement (e.g. on core 14WLL-2A at the tube coupling where density measurements are not directly comparable due to doubled tube thickness, at the top and bottom 3 cm of each core section, 2A-1 and 2A-2, and the bottom ~5 cm of core 12WLL-1C) are not presented here (see main text, Fig. 2). To assess preservation of stratigraphy in the deepest sediments, core 14WLL-2A was imaged at The Field Museum using digital x-radiography at a resolution of ca. 200 dpi (Fig. S1).

Core Dating. ^{14}C ages were calibrated to cal yr BP using CALIB html version 7.1 (1) and the IntCal13 calibration curve (2) (Table S1). A live aquatic moss recovered from WLL with an Ekman dredge in 2014 yielded a post-bomb ("modern") age. Dating by optically stimulated luminescence (OSL) was attempted, but quartz content in core material was too low for traditional OSL methods.

^{10}Be Dating. Quartz was isolated and beryllium extracted from the 250-710 μm fraction of crushed, sieved samples following methods modified from Schaefer et al. (2009) (3). Ages were calculated as described in Methods (see main text) and using time-invariant scaling (4–6) (i.e., "St" scaling; other scaling methods result in a less than 2% difference in ^{10}Be ages) (Fig. S2, Table S2).

Glaciolacustrine "Gray Mud" Units. WLL sediments are organic-rich brown muds with abundant aquatic moss macrofossils, except for two discrete inorganic gray, fine-grained mud layers (one each within the Holocene and pre-LGM sediments) which have the appearance of glaciolacustrine sediments. The timing of deposition of the Holocene gray mud layer (constrained by ^{14}C to between 3.5 and 2.4 ka; see main text, Fig. 2) corresponds with nearby advances between ~3.2 and 2.1 ka of Tunge and Nuna Rampen, two lobate outlet glaciers of the Greenland Ice Sheet that dammed the adjacent glacial lake Nordsø (for location of Nordsø, see Fig. S2) by blocking its outlet (7). Their advance created a larger, deeper Nordsø glacial lake, evidenced by a system of higher shorelines around the modern lake Nordsø (7), and we infer that the enlarged glacial lake Nordsø temporarily flooded WLL. During this brief period of distal glaciofluvial input to WLL via Nordsø, midge assemblages were affected by greater water depth, increased turbidity and input of cold water in the summer. Therefore, we mark assemblages from this unit, and a similarly composed gray mud layer in the LIG, as not necessarily accurately recording summer air temperatures (see main text, Fig. 3).

Midges. Midge subfossil preparation followed protocols described by Walker et al. (2001) (8). Aliquots of wet sediment (0.1-1 g) were deflocculated in 100 ml of 5% KOH at 75°C for twenty minutes. Sediment was sieved using 106 μm mesh. Head capsules and mandibles were then hand-picked from suspended bulk material in a Bogorov tray and mounted with Euparal. Midge larvae are aquatic and shed morphologically distinct chitinous head capsules during ecdysis which are often well preserved in lake sediments. Surveys of modern midge assemblages show a strong relationship between midge distribution and summer air temperature (9). Consequently,

quantitative transfer functions for inferring paleotemperature from subfossil assemblages are used in many Arctic and sub-Arctic regions including North America and Scandinavia (10–14). This method may be especially well-suited for reconstructions of the late Quaternary in very high-latitude regions where soil and vegetation development, and thus secondary environmental controls, are limited (15, 16). Most relevant to this study, midges have been used to infer Holocene temperatures in several lakes in east and west Greenland (16–18) and LIG temperatures in three lakes on Baffin Island and one in Denmark (10, 19, 20).

Midge head capsules are abundant (concentrations range from ~100 to 1200 g^{-1} wet sediment) and well preserved in the sediments of WLL. Every head capsule in each sediment sample was picked and enumerated. All samples included in the study yielded a minimum of 50 identifiable, whole head capsules, the standard for quantitative analysis of assemblages (21, 22). Midges were identified to the highest degree of taxonomic certainty using the classification of Brooks et al. (2007) (23) and with Larocque and Rolland (2006) (24) also referenced. WLL subfossil assemblages contain 40 distinct morphotypes, 39 of which (representing >99% of assemblage compositions) are in the training set. After identification, some downcore taxa were lumped into larger taxonomic groups to harmonize with the lower taxonomic resolution of the training set (10). Lumping included all members of the subtribe Tanytarsini, genera of Pentaneurini were lumped as tribe Pentaneurini, *Procladius* and *Macropelopia* were lumped together as *Procladius*-type, and all morphotypes of the following genera or groups of genera were lumped at the genus level: *Chironomus, Cricotopus*/*Orthocladius*, *Heterotrissocladius*, *Hydrobaenus*/*Oliveridia*, *Corynoneura*/*Thienemanniella*, *Eukiefferiella*/*Tvetenia*, *Zalutschia*, and *Psectrocladius*. *Chaoborus* were similarly identified to the genus level and lumped together (Figs. S3, S4, S5). Up to 8% of head capsules in a subfossil community used in temperature reconstructions could not be identified (e.g. had lost morphological ornaments). One taxon, *Diamesa aberrata*, with maximum contribution to the taxonomic composition of <1%, is not represented in the Francis et al. (2006) training set and thus was not utilized in temperature reconstructions or in Fig. 3 (main text). Our maximum peak early Holocene temperature estimate is derived from averaging the three consecutive temperature reconstructions between 10-8 ka and the anomaly for this period is generated by subtracting the modern (AD 1952-2014 climate norm) July air temperature value of 6.2°C (25) from that average. Our minimum peak LIG temperature estimate was similarly derived from averaging the warmest three consecutive temperature reconstructions in the unit below the hiatus, and the LIG peak anomaly was found by subtracting 6.2°C from that average.

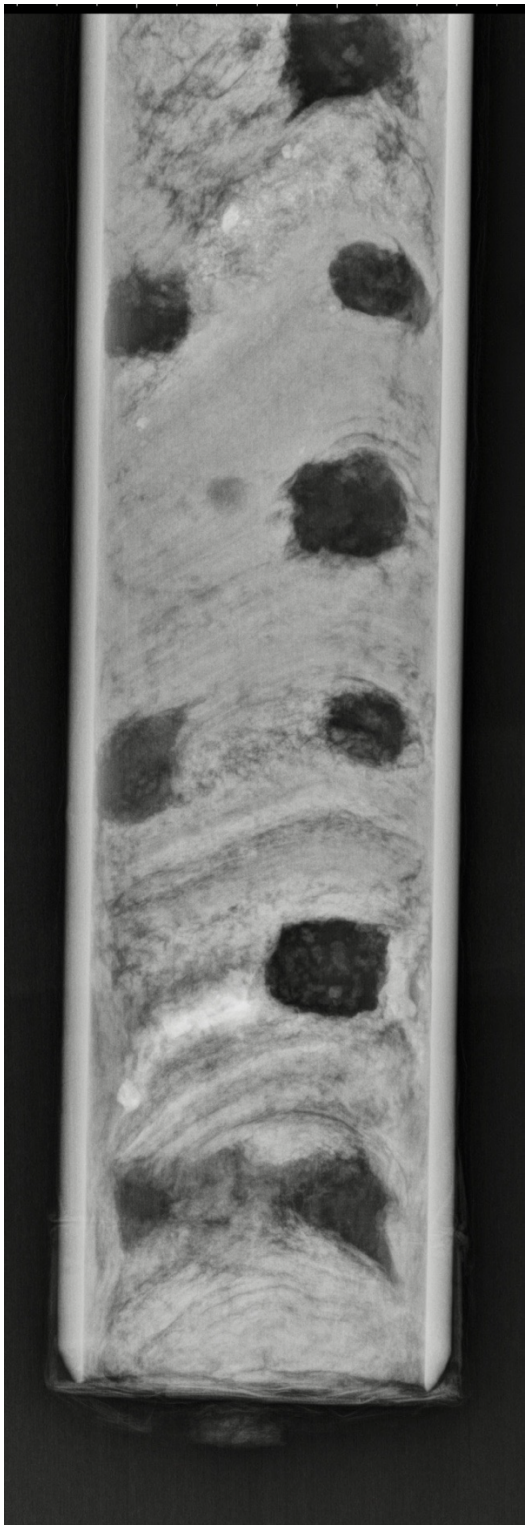

Fig. S1. X-radiograph of sampled basal sediments of core 14WLL-2A, demonstrating the laminated nature of the deepest LIG sediments (dark areas disrupting the stratigraphy are holes created by sampling).

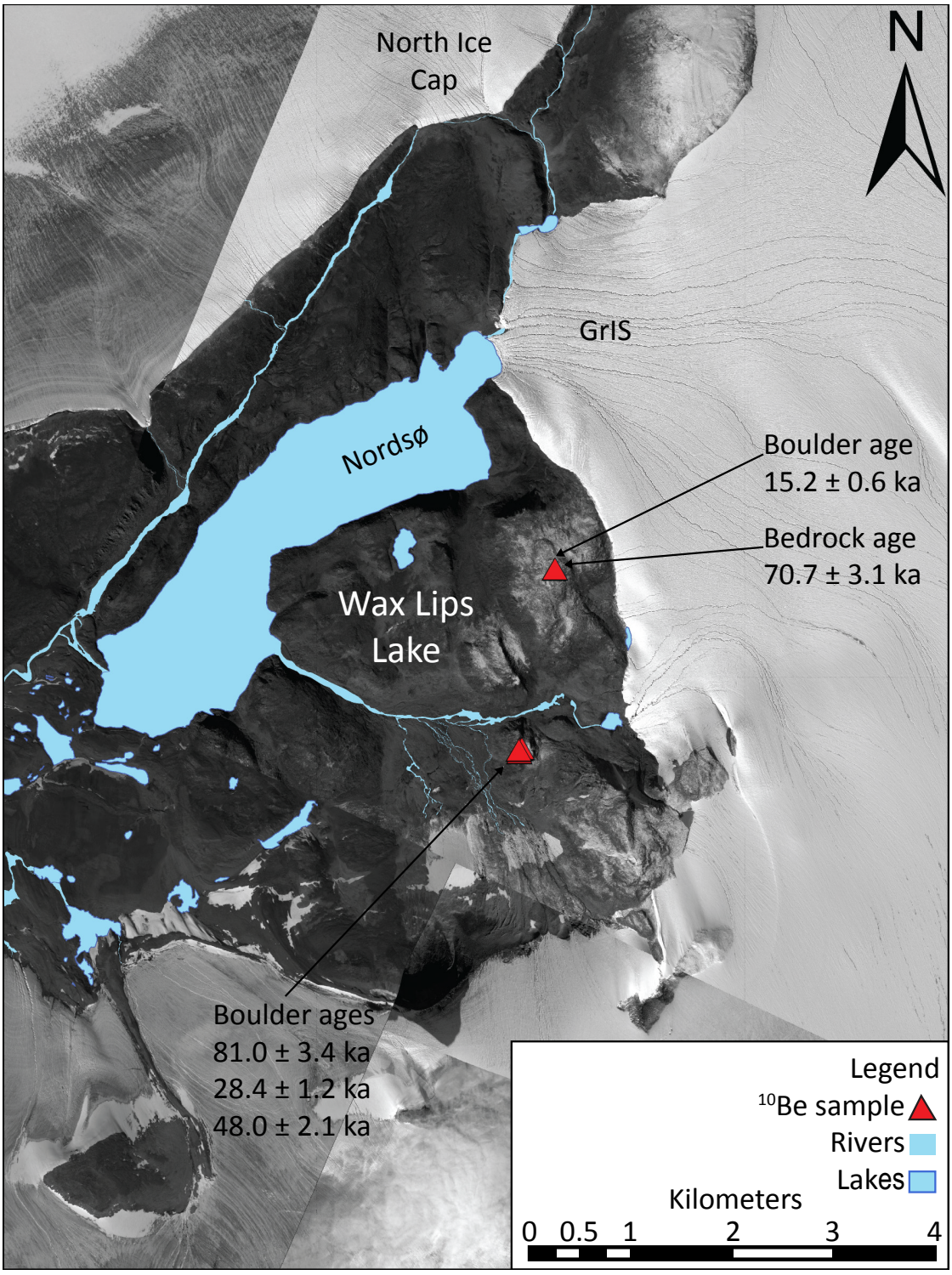

Fig. S2. ^{10}Be ages of exposed bedrock surfaces and perched boulders associated with the weathered drift surrounding WLL. Also shown are locations of WLL, the nearby glacial lake Nordsø, and the present-day GrIS. Worldview 1 and 2 satellite imagery was collected in 2010 and 2012.

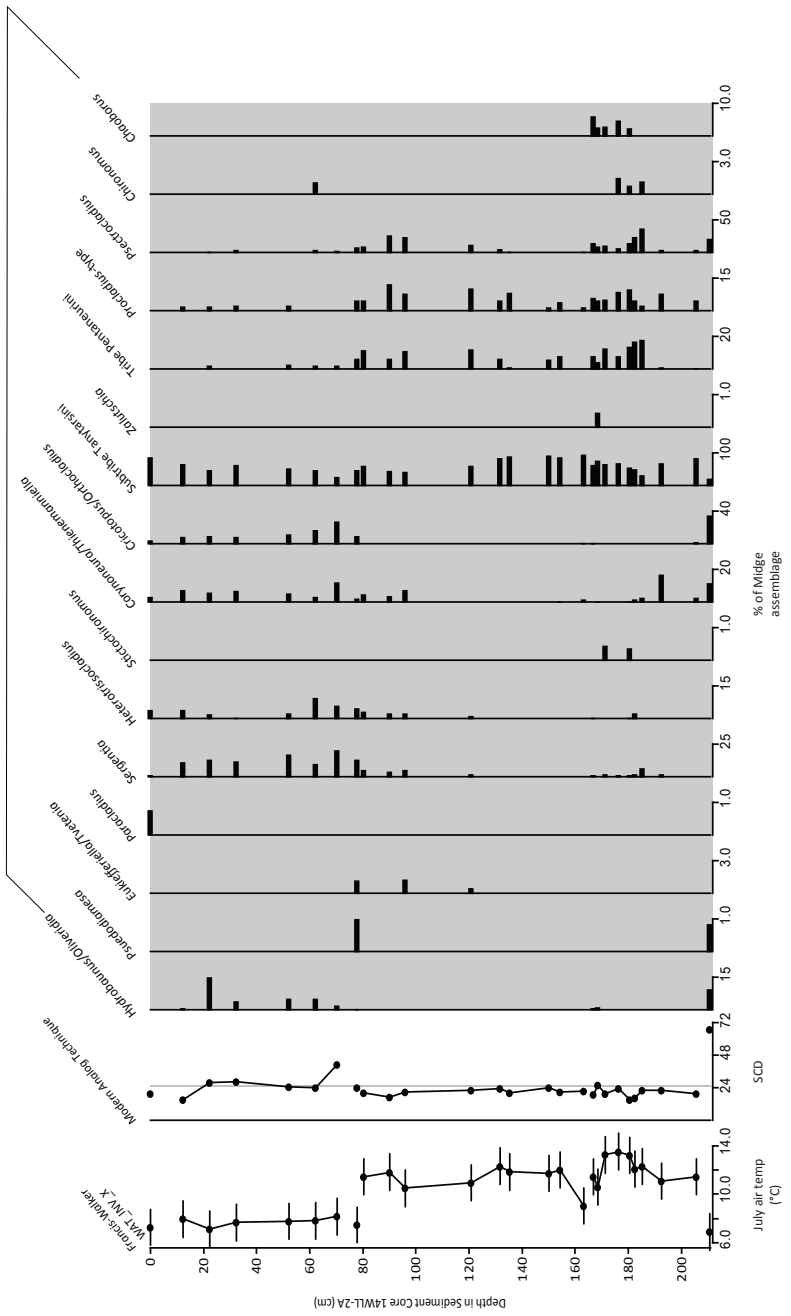

Fig. S3. Standard biostratigraphic diagram showing modeled temperatures (modeled as described in the paper text, using C2 (26)); squared chord distances (SCD) for subfossil assemblages relative to the training set (10), with 5th percentile of the modern training set represented by gray vertical line; and percentages of enumerated taxa.

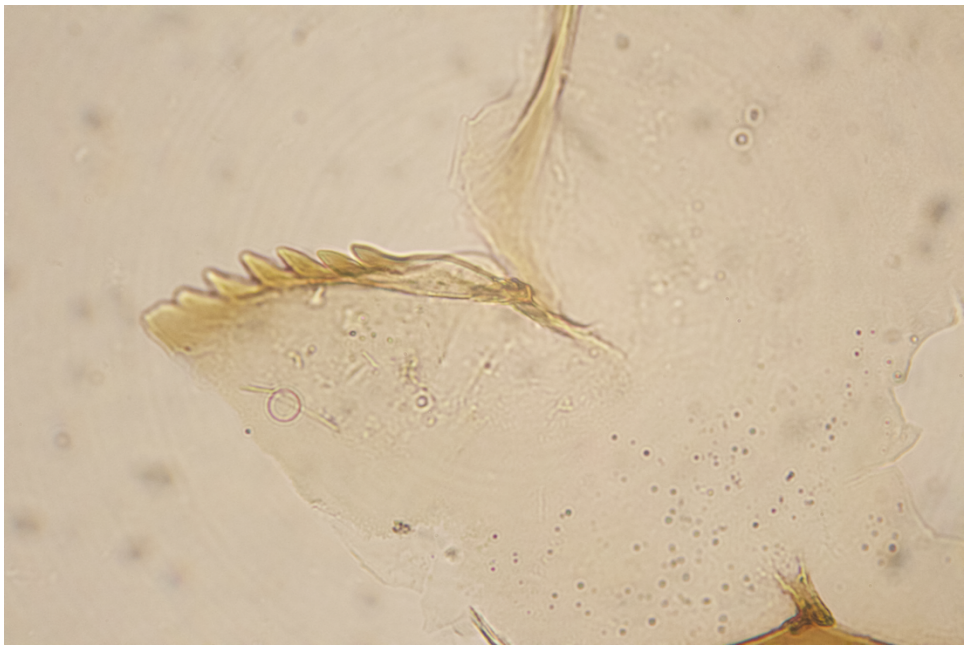

Fig. S4. Half head capsule of *Hydrobaenus/Oliveridia* from Holocene sediments of WLL

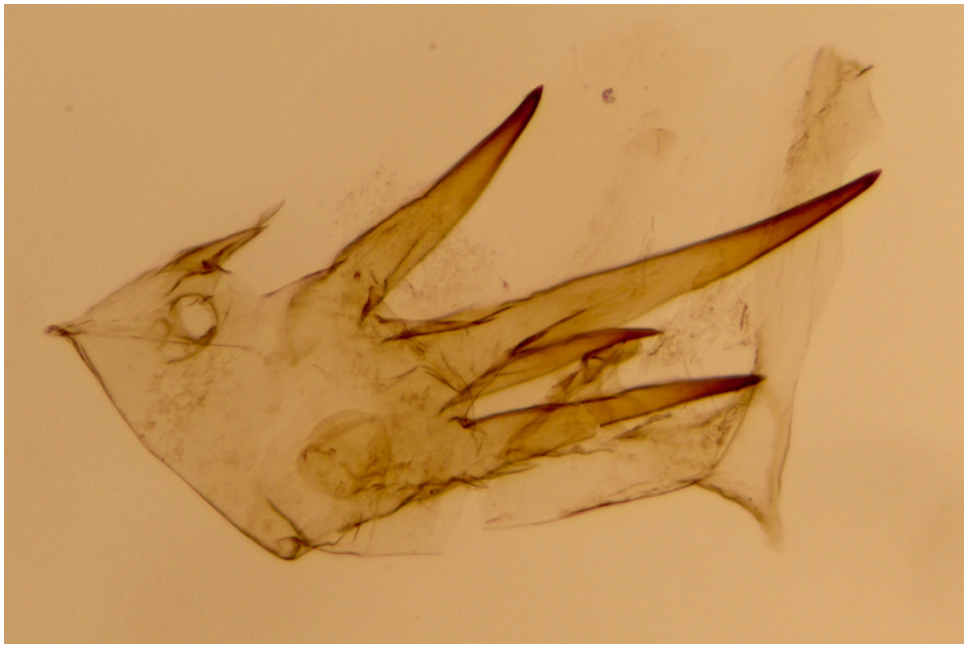

Fig. S5. *Chaoborus* mandible from LIG sediments of WLL

Table S1. Radiocarbon ages

Targets prepared and measured at Woods Hole Oceanographic Institution and calibrated using IntCal13v7.1 (1)

Source	Material Dated	Depth in Section (cm)	Composite Core Depth (cm)	Fraction Modern	$\delta^{13}C$ (‰)	Radiocarbon Age (^{14}C yr BP)	Calibrated Age (2σ cal yr BP)
Ekman dredge							
14WLL-N1-E	Living aquatic moss			1.1685±0.0025	-24.92	>modern	modern
14WLL-U1-E2	Aquatic moss			0.9283±0.0020	-20.37	595±15	546-644
Sediment cores							
14WLL-2A-1	Aquatic moss	5-6	5.5	0.9078±0.0019	-22.01	775±15	677-726
14WLL-2A-1	Aquatic moss	24-25	24.5	0.8609±0.0017	-22.18	1200±15	1070-1177
14WLL-2A-1	Aquatic moss	47-48	47.5	0.8612±0.0017	-22.24	1200±15	1070-1177
14WLL-2A-1	Aquatic moss	56-57	56.5	0.7783±0.0017	-22.54	2010±15	1903-1995
14WLL-2A-2	Aquatic moss	5-6	70.5	0.7454±0.0023	-21.43	2360±25	2337-2458
14WLL-2A-2	Aquatic moss	29.5-30.5	95	0.6001±0.0016	-19.89	4100±20	4526-4803
14WLL-2A-2	Aquatic moss	66.5-67.5	132	0.4086±0.0016	-20.85	7190±30	7946-8049
14WLL-2A-2	Aquatic moss	93.5-94.5	159	0.3317±0.0017	-26.56	8870±40	9783-10173
14WLL-2A-2	Aquatic moss	115.5-116.5	181	0.0019±0.0021	-22.18	>44400	non-finite
14WLL-2A-2	Aquatic moss	145.5-146.5	211	-0.0005±0.0005	-21.59	>48000	non-finite
12WLL-1A	Aquatic moss	2-2.5	2.25	0.652±0.0029	-20.84	3440±35	3611-3828
12WLL-1A	Aquatic moss	14.5-15	14.75	0.5819±0.0020	-21.48	4350±25	4853-4972
12WLL-1A	Aquatic moss	22.5-23	22.75	0.3252±0.0016	-25.48	9020±40	9967-10248
12WLL-1A	Aquatic moss	40.5-41	40.75	0.4894±0.0031	-21.44	5740±50	6414-6656
12WLL-1A	Aquatic moss	44-44.5	44.25	-0.0039±0.0029	-22.23	>44200	non-finite
12WLL-1C	Aquatic moss	1.5	1.5	0.6641±0.0022	-21.2	3290±25	3457-3571
12WLL-1C	Aquatic moss	30	30	0.5332±0.0021	-23.66	5050±30	5726-5901
12WLL-1C	Aquatic moss	45.5	45.5	0.4286±0.0025	-22.36	6810±45	7578-7718
12WLL-1C	Aquatic moss	50	50	0.0265±0.0016	-23.63	29200±470	32735-33919
12WLL-1C	Aquatic moss	54.5	54.5	0.0028±0.0008	-23.42	47300±2200	non-finite

Table S2. ^{10}Be ages of samples of bedrock and boulders associated with weathered drift
[a]Samples were measured with beryllium standard 07KNSTD (Nishiizumi K, et al. 2007) (27)
[b]Uncertainty is internal AMS uncertainty
***Sample taken from bedrock**

	Lat. (ºN)	Long. (ºW)	Elevation (m a.s.l.)	Thickness (cm)	Shielding Correction	^{10}Be Conc.[a] (atoms/g)	Uncertainty[b] (atoms/g)	Age ± uncertainty
NT-14-1	76.8389	-66.887	618	4.48	0.999	3.65E+05	6.59E+03	48,040 ± 2050
NT-14-2	76.8391	-66.8861	614	4.43	0.995	6.06E+05	1.01E+04	80,970 ± 3440
NT-14-4	76.8387	-66.8864	614	5.69	0.999	2.14E+05	4.17E+03	28,410 ± 1230
NT-14-5	76.8552	-66.9005	722	5.77	1	1.27E+05	2.24E+03	15,170 ± 640
NT-14-6*	76.8552	-66.9005	722	2.75	1	5.98E+05	1.16E+04	70,670 ± 3080

Table S3. WLL core locations

Core	Coring system	Lat. (ºN)	Long. (ºW)	Water depth at core site (m)	Core length (m)
12WLL-1A	Modified-Bolivia	76.85205	-66.9598	8.25	0.70
12WLL-1C	Modified-Bolivia	76.85212	-66.9595	8.20	0.67
14WLL-2A	Nesje	76.85184	-66.9592	7.19	2.16

References

1. Stuiver M, Reimer PJ, Reimer RW (2017) CALIB 7.1 [WWW program]. Available at: http://calib.org [Accessed May 1, 2017].
2. Reimer PJ, et al. (2013) IntCal13 and Marine13 radiocarbon age calibration curves 0–50,000 Years cal BP. *Radiocarbon* 55(4):1869–1887.
3. Schaefer JM, et al. (2009) High-frequency Holocene glacier fluctuations in New Zealand differ from the northern signature. *Science* 324(5927):622–625.
4. Balco G, Stone JO, Lifton NA, Dunai TJ (2008) A complete and easily accessible means of calculating surface exposure ages or erosion rates from ^{10}Be and ^{26}Al measurements. *Quat Geochronol* 3:174–195.
5. Lal D (1991) Cosmic ray labeling of erosion surfaces: in situ nuclide production rates and erosion models. *Earth Planet Sci Lett* 104:424–439.
6. Stone JO (2000) Air pressure and cosmogenic isotope production. *J Geophys Res* 105(B10):23753–23759.
7. Farnsworth LB, et al. (2018) Holocene history of the Greenland Ice Sheet margin in northern Nunatarssuaq, northwest Greenland. *Arktos J Arct Geosci* 4:10. doi: 10.1007/s41063-018-0044-0
8. Walker IR (2001) Midges: Chironomidae and Related Diptera. *Tracking Environmental Change Using Lake Sediments. Volume 4: Zoological Indicators*, eds Smol JP, Birks HJB, Last WM (Kluwer Academic Publishers, Dordrecht, The Netherlands), pp 43–66.
9. Walker IR, Levesque AJ, Cwynar LC, Lotter AF (1997) An expanded surface-water palaeotemperature inference model for use with fossil midges from eastern Canada. *J Paleolimnol* 18(2):165–178.
10. Francis DR, Wolfe AP, Walker IR, Miller GH (2006) Interglacial and Holocene temperature reconstructions based on midge remains in sediments of two lakes from Baffin Island, Nunavut, Arctic Canada. *Palaeogeogr Palaeoclimatol Palaeoecol* 236(1–2):107–124.
11. Barley EM, et al. (2006) A northwest North American training set: distribution of freshwater midges in relation to air temperature and lake depth. *J Paleolimnol* 36(3):295–314.
12. Fortin M-C, et al. (2015) Chironomid-environment relations in northern North America. *J Paleolimnol* 54(2–3):223–237.
13. Langdon PG, Holmes N, Caseldine CJ (2008) Environmental controls on modern chironomid faunas from NW Iceland and implications for reconstructing climate change. *J Paleolimnol* 40(1):273–293.
14. Brooks SJ (2006) Fossil midges (Diptera: Chironomidae) as palaeoclimatic indicators for the Eurasian region. *Quat Sci Rev* 25(15–16):1894–1910.
15. Brooks SJ, Axford Y, Heiri O, Langdon PG, Larocque-Tobler I (2012) Chironomids can be reliable proxies for Holocene temperatures. A comment on Velle et al. (2010). *The Holocene* 22(12):1495–1500.
16. Axford Y, et al. (2017) Timing and magnitude of early to middle Holocene warming in East Greenland inferred from chironomids. *Boreas* 46(4):678–687.
17. Axford Y, et al. (2013) Holocene temperature history at the western Greenland Ice Sheet margin reconstructed from lake sediments. *Quat Sci Rev* 59:87–100.
18. Wooller MJ, et al. (2004) Quantitative paleotemperature estimates from δ^{18}O of chironomid head capsules preserved in arctic lake sediments. *J Paleolimnol* 31(3):267–274.
19. Axford Y, et al. (2011) Chironomids record terrestrial temperature changes throughout Arctic interglacials of the past 200,000 yr. *Bull Geol Soc Am* 123(7–8):1275–1287.
20. Jones RT, et al. (2017) Delayed maximum northern European summer temperatures

during the Last Interglacial as a result of Greenland Ice Sheet melt. *Geology* 45(1):23–26.
21. Heiri O, Lotter AF (2001) Effect of low count sums on quantitative environmental reconstructions: an example using subfossil chironomids. *J Paleolimnol* 26(3):343–350.
22. Larocque I (2001) How many chironomid head capsules are enough? A statistical approach to determine sample size for palaeoclimatic reconstructions. *Palaeogeogr Palaeoclimatol Palaeoecol* 172(1–2):133–142.
23. Brooks SJ, Langdon PG, Heiri O (2007) *The Identification and Use of Palaearctic Chironomidae Larvae in Palaeoecology* (Quaternary Research Assocation, London, UK).
24. Larocque I, Rolland N (2006) *A Visual Guide to Sub-fossil Chironomids from Quebec to Ellesmere Island* (Institut National de la Recherche Scientifique, Québec).
25. Wong GJ, et al. (2015) Coast-to-interior gradient in recent northwest Greenland precipitation trends (1952–2012). *Environ Res Lett* 10(11):114008.
26. Juggins S (2007) C2 Version 1.7.7: software for ecological and paleoecological data analysis and visualisation.
27. Nishiizumi K, et al. (2007) Absolute calibration of ^{10}Be AMS standards. *Nucl Instruments Methods Phys Res Sect B Beam Interact with Mater Atoms* 258(2):403–413.